Lubrication at the Frontier / D. Dowson et al. (Editors)

Amplitude Reduction of Non-Isotropic Harmonic Patterns in Circular EHL Contacts, under Pure Rolling

C.H. Venner[a], A.A. Lubrecht[b]

[a]University of Twente, Enschede, The Netherlands.

[b]Laboratoire de Mécanique des Contacts, UMR CNRS 5514, INSA de Lyon, France.

Surface roughness plays an important role in ElastoHydrodynamically Lubricated contacts, a role which is currently only partially understood. Recent work on waviness in EHL line contacts has shown and quantified the elastic deformation of the waviness inside the contact as a function of a single dimensionless parameter. In the present paper this work is extended to the circular contact problem. First it is shown that the amplitude reduction of an isotropic harmonic pattern can also be described as a function of a single dimensionless parameter. Subsequently, the effects of anisotropy are investigated varying from purely transverse to purely longitudinal. It is shown that one can create a single curve for the case varying from isotropic to longitudinal, and another for the case varying from isotropic to transverse. Both curves can be combined in a single formula.

1. Introduction

Tendencies in design are such that EHL contacts are required to operate reliably under increasingly severe conditions, e.g. higher loads, higher temperatures, sparser lubricant supply. As a result the film thickness in the contact will be smaller, and the microgeometry of the surface has an increased effect on the operation of the contact. In fact, the microgeometry or surface roughness can no longer be seen as a given feature. On the contrary, surface texture is rapidly becoming a design parameter too. Finally environmental awareness calls for silent machinery and thus silent bearings. This requires detailed understanding of the different sources of vibrations, and of the dynamic behaviour of the individual EHL contacts and its relation with the microgeometry. Summarizing, a detailed understanding of the effects of microgeometry on film formation and surface deformation is as important as ever before.

The study of effects of surface features in EHL contacts has a long history, both experimentally and theoretically, e.g. see [1]. Experimental results can be found in [2]-[7]. Theoretical studies mostly addressed the subject by means of numerical simulations. The steady state problem was studied first, e.g. see [8]-[16]. Examples of transient studies of the pressure and film thickness are [17]-[31]. Most of these studies deal with a surface feature on one of the surfaces. Results for two non-smooth surfaces can be found e.g. in [32] and [33].

Obviously for non-smooth surfaces generally dense grids are required to obtain accurate results. Moreover, from a stability point the rough surface problem tends to be more demanding than the smooth surface problem. Finally, by definition, in the case of roughness on a moving surface the problem becomes transient. Consequently, fast and stable algorithms for the numerical solution of the problem are a prerequisite for such studies. These algorithms were long lacking. However, the situation has changed with the introduction and further development of so-called multigrid or multilevel techniques by Lubrecht [34]-[36], and Venner [37].

An alternative approach to full numerical simulations was pioneered by Greenwood et al. [38]-[41]. They showed that transient EHL solutions consist in principle of two parts; a particular integral (moving steady state solution with the velocity of the rough surface) and a complementary function (excitation coming from the inlet) travelling with the average velocity of the lubri-

cant, and thereby resulting in film changes with a wavelength that is larger or smaller than the wavelength of the undeformed waviness.

It thus appears that the basic phenomena involved in transient EHL contacts are relatively well understood nowadays. The necessary next step is to generalise the results to obtain tools for practical use in e.g. design. A first step in this direction was taken by Couhier [42] and Venner et al. [43]. It was shown that the numerical results of the amplitude reduction of waviness in an EHL line contact under pure rolling could be represented on a "master-curve" of a single dimensionless parameter. Such a curve obviously can form an important tool to estimate deformation of rough surfaces, i.e. by applying it to each of the Fourier components of the surface, and then by inverse Fourier transform construct the deformed film thickness. Subsequently, the mastercurve was extended to include the effects of sliding in [44]. Theoretical support for the observed behaviour was provided recently by Hooke [45].

In the present paper the approach is extended to the circular contact problem. By means of numerical simulations the amplitude reduction of harmonic surface patterns is investigated for conditions of pure rolling.

2. Nomenclature

a	amplitude
A	dimensionless amplitude $A = aR/b^2$
b	radius of Hertzian contact $b = \sqrt[3]{(3FR_x)/(2E')}$
E'	reduced modulus of elasticity $2/E' = (1-\nu_1^2)/E_1 + (1-\nu_2^2)/E_2$
F	external load
G	dimensionless materials parameter $G = \alpha\, E'$
h	film thickness
H	dimensionless film thickness $H = hR_x/b^2$
L	dimensionless material parameter (Moes) $L = G(2U)^{0.25}$
M	2d dimensionless load parameter (Moes) $M = W(2U)^{-0.75}$
p	pressure
p_h	maximum Hertzian pressure $p_h = (3F)/(2\pi b^2)$
P	dimensionless pressure $P = p/p_h$
R_x	reduced radius of curvature in x $1/R_x = 1/R_{1x} + 1/R_{2x}$
R_y	reduced radius of curvature in y $R_y = R_x$
$\mathcal{R}$	surface feature
S	slip parameter $S = u_1/\bar{u}$
T	dimensionless time $T = t\bar{u}/b$
u	surface velocity
$\bar{u}$	mean velocity $\bar{u} = (u_1 + u_2)/2$
U	dimensionless speed parameter $U = (\eta_0\bar{u})/(E'R_x)$
W	2d dimensionless load parameter $W = F/(E'R_x^2)$
x	coordinate in direction of rolling
X, X'	dimensionless coordinate $X = x/b$
$\bar{X}$	dimensionless location surface feature
y	coordinate perpendicular to x
Y, Y'	dimensionless coordinate $Y = y/b$
α	pressure viscosity index
ϵ	coefficient in Reynolds' equation $\epsilon = (\bar{\rho}H^3)/(\bar{\eta}\bar{\lambda})$
Δ_T	dimensionless time step
Δ_X, Δ_Y	dimensionless mesh size in X, Y
∇_2	dimensionless wavelength parameter $\nabla_2 = (\lambda/b)(M^{1/2}/L^{1/2})$
$\bar{\lambda}$	dimensionless speed parameter $\bar{\lambda} = 12(\eta_0\bar{u}R_x^2)/(b^3p_h)$
λ_x,λ_y	wavelength in x, y direction
η	viscosity
$\bar{\eta}$	dimensionless density $\bar{\eta} = \eta/\eta_0$
ρ	density
$\bar{\rho}$	dimensionless density $\bar{\rho} = \rho/\rho_0$
subscripts	
a,b	inlet, outlet
i,d	initial (undeformed), deformed
s	start
0	constant, e.g. at ambient pressure
1,2	surface 1, 2

3. Theory

The dimensionless Reynolds equation for the transient circular contact problem reads:

$$\frac{\partial}{\partial X}\left(\epsilon\frac{\partial P}{\partial X}\right)+\frac{\partial}{\partial Y}\left(\epsilon\frac{\partial P}{\partial Y}\right)-\frac{\partial(\bar{\rho}H)}{\partial X}-\frac{\partial(\bar{\rho}H)}{\partial T}=0(1)$$

The boundary conditions are $P(X_a,Y,T) = P(X_b,Y,T) = P(X,Y_a,T) = P(X,Y_b,T) = 0$, $\forall T$ where X_a, X_b, Y_a and Y_b denote the boundaries of the domain. Furthermore, the cavitation condition $P(X,Y,T) \geq 0$, $\forall X,Y,T$ must be satisfied. ϵ and $\bar{\lambda}$ are defined according to:

$$\epsilon = \frac{\bar{\rho}H^3}{\bar{\eta}\bar{\lambda}} \qquad \bar{\lambda} = \frac{12\eta_0\bar{u}R_x^2}{b^3p_h}$$

The density ρ is assumed to depend on the pressure according to the Dowson and Higginson relation [46] and the Roelands viscosity pressure relation [47] is used.

The film thickness equation is made dimensionless using the same Hertzian parameters and accounting for a moving surface pattern $\mathcal{R}$ reads:

$$H(X,Y,T) = H_0(T) + \frac{X^2}{2} + \frac{Y^2}{2} - \mathcal{R}(X,Y,T) + \frac{2}{\pi^2}\int_\Omega \frac{P(X',Y',T)\,dX'\,dY'}{\sqrt{(X-X')^2+(Y-Y')^2}} \quad (2)$$

where $\mathcal{R}(X,Y,T)$ denotes the undeformed geometry of the surface feature at dimensionless time T and $H_0(T)$ is an integration function. In this paper calculational results will be presented for isotropic and non isotropic harmonic surface patterns. This pattern is assumed to be located on the surface moving with velocity u_1 and modelled according to:

$$\mathcal{R}(X,Y,T) = A_i\, 10^{-10(\max(0,\frac{X-\bar{X}}{(\lambda_x/b)})^2)} \cos\left(2\pi\frac{X-\bar{X}}{(\lambda_x/b)}\right)\cos\left(2\pi\frac{Y}{(\lambda_y/b)}\right) \quad (3)$$

where $\bar{X} = X_s + ST$ with $S = u_1/\bar{u}$. This particular shape was chosen to avoid discontinuous derivatives, and to start the calculation with a smooth surface geometry.

At all times the force balance condition is imposed, i.e. the integral over the pressure must balance the externally applied contact load. This condition determines the value of the integration function $H_0(T)$ in equation (2). Expressed in the dimensionless variables it reads:

$$\int_\Omega P(X,Y,T)\,dX\,dY - \frac{2\pi}{3} = 0, \quad \forall T \quad (4)$$

In physical terms this equation means that the acceleration forces of the contacting bodies are neglected.

We will determine the deformed amplitude of the pattern as a function of the operating conditions:

$$2A_d = \max_T H(0,0,T) - \min_T H(0,0,T) \quad (5)$$

This definition is suited for all cases except for purely longitudinal waviness $\lambda_x = \infty$. For that case it needs to be generalised as will be explained in Sec. 5.3.

4. Numerical Solution

The equations were discretised on a uniform grid with second order accuracy in space and time. The discrete equations are the same as used in [48] except for the discretisation of the wegde and squeeze term. For these terms an alternative scheme was used adopted from Computational Fluid Dynamics, and referred to as $NU2$ (Narrow Upstream 2nd order). Unlike the usual approach where each of the *advective* terms $(\bar{\rho}H)_X$ and $(\bar{\rho}H)_T$ is discretised separately using backwards (upstream, upwind) second order discretisation ($SU2$), the combined term $(\bar{\rho}H)_X + (\bar{\rho}H)_T$ is considered. The resulting scheme is still second order, but as the leading term of its truncation error vanishes for two directions $X = T$ and $X = 2T$, (instead of only for $X = T$) the truncation error for other components is generally smaller too. This scheme was tested for the line contact problem showing a significantly higher accuracy for small wavelengths, see [33]. Also for the circular contact problem it yields a significant increase in accuracy as is illustrated in appendix A.

The discrete equations per time step were solved using multilevel techniques to accelerate convergence of the relaxation process. Unlike [48] the techniques were directly applied to the second

order equations and double discretisation was not used. The elastic deformation integrals were computed using Multilevel Multi-Integration. For the basic techniques involved the reader is referred to [34] and [37].

The calculations were performed using a domain $-2.5 \leq X \leq 1.5$ and $-2 \leq Y \leq 2$ using a grid with 257×257 points. The time step was chosen equal to the spatial mesh size, i.e. with $\Delta_T = \Delta_X = \Delta_Y = 0.015625$. As we are interested in small amplitude waviness the amplitude of the undeformed wave was taken as 20 % of the central film thickness obtained when assuming perfectly smooth surfaces. The simulation was started with the $X_s = -2.5$. Subsequently the pattern moves into the contact with the velocity of the wavy surface. Monitoring of the central film thickness to determine A_d is started at $T = T_s$ where T_s denotes the time after which the solution has become periodic, i.e. when all running in effects have disappeared. To obtain a time independent value for A_d it is important that monitoring only starts for $T > T_s$. As a general rule T_s can be taken as the time at which the slowest of the induced or real wave reaches the end of the contact. Subsequently the monitoring time should be taken sufficiently long to ensure that a real maximum and minimum have occured. As we assume pure rolling in the present paper it is sufficient to have a monitoring time that is (a multiple of) λ_x/b.

5. Results

The behaviour of the reduced amplitude A_d was studied as a function of the dimensionless wavelengths λ_x/b, λ_y/b and the operating conditions M, L. Below the results are presented organized according to the pattern orientation. First in section 5.1 results for the isotropic case $\lambda_x = \lambda_y = \lambda$ are presented. Subsequently in the sections 5.2 and 5.3 the cases $\lambda_x < \lambda_y$ (including the transverse limit) and $\lambda_x > \lambda_y$ (including the longitudinal limit) are discussed.

5.1. Isotropic: $\lambda_x = \lambda_y = \lambda$

Figure 1 shows the pressure and film thickness as a function of X and Y for a typical case. The conditions are $M = 1007.6$, $L = 12.05$ and $\lambda/b = 0.25$. With $\alpha = 2.2\ 10^{-8}$ the maximum Hertzian pressure for this case is $p_h = 2.0\ GPa$. The undeformed amplitude was taken as $A_i = 5.6\ 10^{-3} = 0.2H_c$ with H_c the smooth surface central film thickness. The value of A_d obtained for this case is $A_d = 4.136\ 10^{-3} = 0.739\ A_i$.

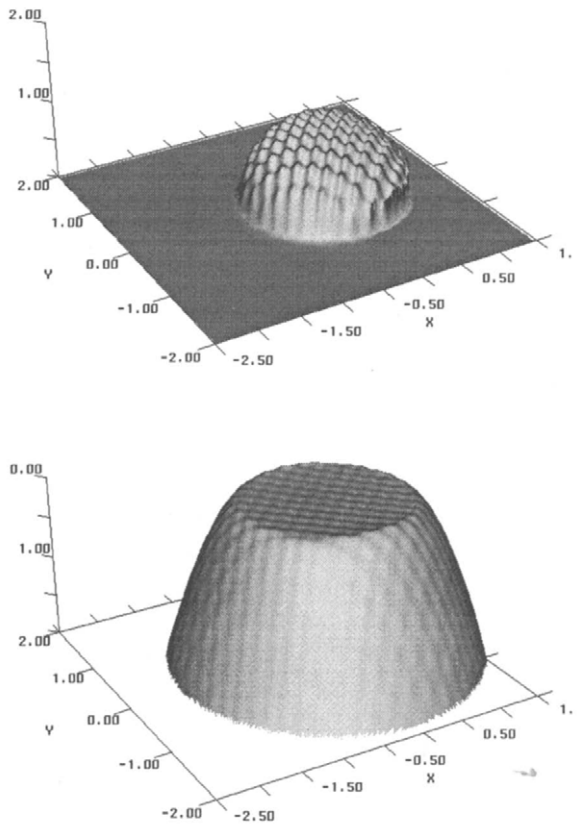

Figure 1. *Snapshot of P (top) and H (bottom) as a function of X and Y, under pure rolling* $\lambda = b/4$, $A_i = 0.2H_c$, $M = 1007.6$, $L = 12.05$.

In the same way as for the line contact problem, see Venner et al. [43] and Lubrecht et al. [44], the reduced amplitude A_d was studied as a function of wavelength and operating conditions. First it was established that the results are linear in A_i,

i.e. A_i can be fixed and need not be varied separately. For the line contact this linearity remained valid even for very large values of A_i. For the point contact however, the linearity breaks down when $A_i \approx H_c$. As mentioned earlier, all results presented here were obtained using $A_i = 0.2H_c$.

In a preliminary study [49] it was shown that for a range of M, L and λ/b values, all results fell quite well on a single curve if they were presented as a function of the dimensionless parameter $\nabla_2 = (\lambda/b)(M^{1/2}/L^{\gamma})$ with $1/6 \leq \gamma \leq 1/2$. On physical grounds $\nabla_2 = (\lambda/b)(M^{1/2}/L^{1/2})$ was chosen because it results in the same dependence on $\bar{u}$ and p_h as in the line contact problem, as suggested by Drs Hooke and Greenwood [50]. Note that ∇_2 can be written as $\nabla_2 = \sqrt{2\pi^3/3}\ (\lambda/b)(\alpha\ p_h)^{3/2}\ L^{-2}$.

Fig. 2 presents results of A_d/A_i for isotropic waviness as a function of ∇_2 for cases $50 \leq M \leq 2000$, $L = 12.05$, and $0.125 \leq \lambda/b \leq 4.0$. A two parameter least square fit of the present data shows that the points can be approximated by an equation similar to the one found in the line contact case:

$$\frac{A_d}{A_i} = \frac{1}{1 + 0.15\nabla_2 + 0.015{\nabla_2}^2} \qquad (6)$$

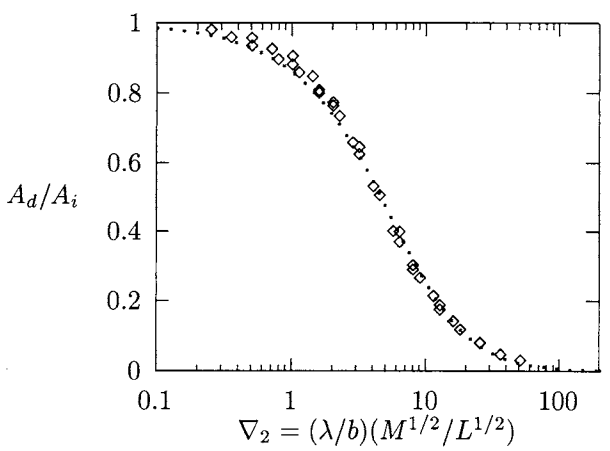

Figure 2. *Relative deformed amplitude as a function of ∇_2, pure rolling. Dotted curve: equation (6).*

5.2. Anisotropic: $\lambda_y > \lambda_x$

Figure 3 shows the pressure and film thickness as a function of X and Y for the same case as considered in Fig. 1 but with $\lambda_y/b = 2\lambda_x/b = 0.50$. For this case the value of the reduced amplitude was $A_d = 4.273\ 10^{-3} = 0.763A_i$

Subsequently, the operating conditions were varied. The question then is which parameter should be used to present the results. As a first guess ∇_2 was chosen with $\lambda = \lambda_x$.

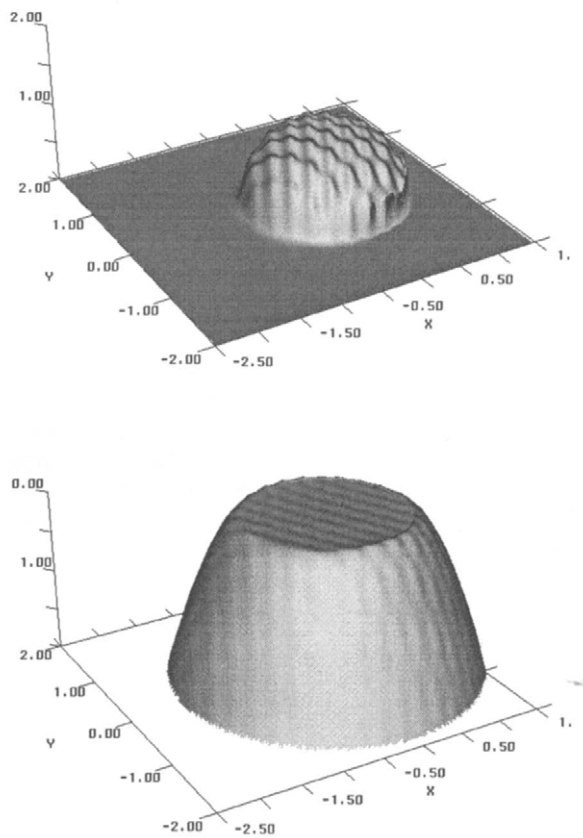

Figure 3. *Snapshot of P (top) and H (bottom) as a function of X and Y, under pure rolling $\lambda_x = b/4$, $\lambda_y = 2\lambda_x$, $A_i = 0.2H_c$, $M = 1007.6$, $L = 12.05$.*

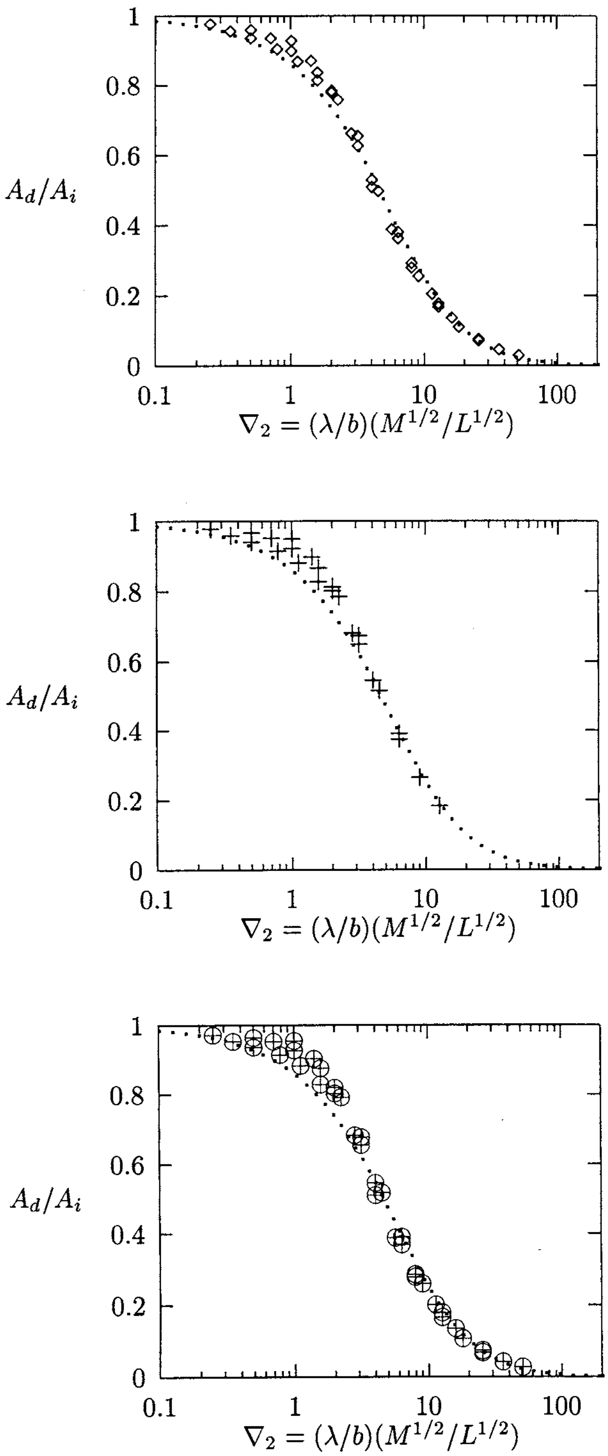

Figure 4. *A_d/A_i as a function of ∇_2 with $\lambda = \lambda_x$. Anisotropic: $\lambda_y/\lambda_x = 2$ (top), 4 (centre) and transverse (bottom).*

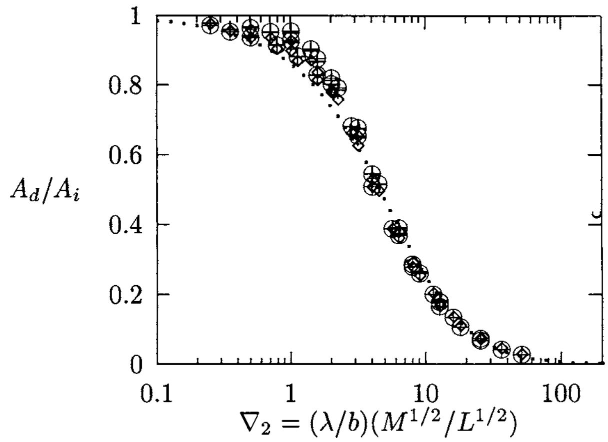

Figure 5. *A_d/A_i as a function of ∇_2 with $\lambda = \lambda_x$. Anisotropic: $\lambda_y > \lambda_x$.*

Figure 4 presents the results obtained for $\lambda_y/\lambda_x = 2$, 4, and for purely transverse, i.e. $\lambda_y = \infty$. For reference the predictions of Eq. (6) are presented. Figure 4 shows that for each ratio λ_y/λ_x the results fall on the curve obtained for the isotropic case. Deviations occur for smaller wavelengths but they seem to be a second order effect. It thus appears that the main behaviour for $\lambda_y > \lambda_x$ is accurately described by Eq. (6) using $\lambda = \lambda_x$ in ∇_2.

This is once more confirmed by Fig. 5 where all results for $\lambda_y > \lambda_x$ are presented in one figure.

5.3. Anisotropic: $\lambda_x > \lambda_y$

Figure 6 shows the pressure and film as a function of X and Y for the same case as considered in Fig. 1 but with $\lambda_y/b = 0.5\lambda_x/b = 0.25$. For this case the value of the reduced amplitude was $A_d = 3.117\ 10^{-3} = 0.557A_i$.

By Eq. (5) the deformed amplitude A_d was defined as half the difference between the maximum value and the minimum value of the film thickness in $X = Y = 0$ taken over time. This implies that with increasing λ_x the required monitoring time increases, i.e. the time before a full period of the oscillation has past. Thus, for the asymptotic case of purely longitudinal waviness ($\lambda_x = \infty$) no result can be obtained. To include this case a generalised definition of A_d is needed. In the

high pressure region the Reynolds equation reduces to a transport equation in the X direction. As in this region the film is nominally flat, the deformed amplitude could also be defined as:

$$2A_d = \max_X H(X,0,T_0) - \min_X H(X,0,T_0) \qquad (7)$$

where the maximum and minimum should be taken over a region of length at least λ_x/b entirely in the high viscosity zone, and T_0 is a time taken after which the contact has settled in the steady oscillation.

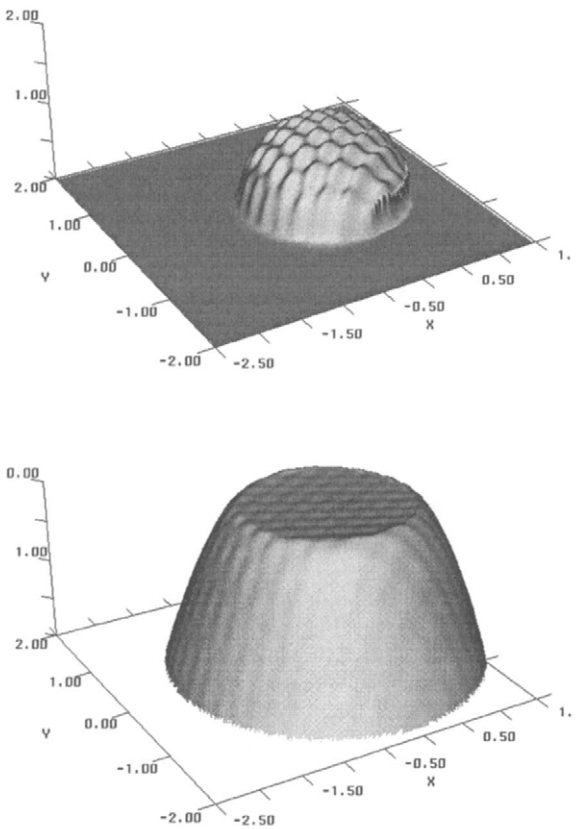

Figure 6. *Snapshot of P (top) and H (bottom) as a function of X and Y, under pure rolling* $\lambda_y = b/4$, $\lambda_x = 2\lambda_y$, $A_i = 0.2H_c$, $M = 1007.6$, $L = 12.05$.

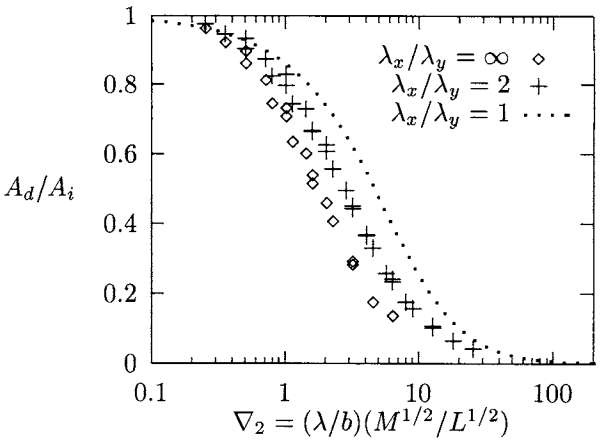

Figure 7. A_d/A_i *as a function of* ∇_2 *with* $\lambda = \lambda_y$, *for* $\lambda_y/\lambda_x = 1, 0.5$, *and longitudinal.*

For $\lambda_x/b < 1$ (7) and (6) should give the same result, i.e. as long as the value determined by (7) is not influenced by the global changes in X direction of the film. For the isotropic case it was also noticed that the amplitude of the film thickness variations in Y direction at a given instance (taken after the solution has settled) was the same as the amplitude in X direction, as long as the wavelength λ_y/b was sufficiently small compared to the size of the contact. Thus it appears that the deformed amplitude could also be taken as:

$$2A_d = \max_{(X,Y)} H(X,Y,T_0) - \min_{(X,Y)} H(X,Y,T_0) \qquad (8)$$

with T_0 as before, and the maximum and minimum taken over a sufficiently large region (at least of size $\lambda_x/b \times \lambda_y/b$, and well inside the high viscosity region, or more specifically well inside the region in which the film thickness for the steady state is nominally flat. For λ_x/b and λ_y/b smaller than unity this generalisation remained valid for anisotropic waviness. Consequently, this generalised definition of A_d was used to study the longitudinal waviness $\lambda_x = \infty$, where it reduces to:

$$2A_d = \max_Y H(X_0,Y,T_0) - \min_Y H(X_0,Y,T_0). \qquad (9)$$

Figure 7 shows A_d/A_i as a function of ∇_2 with λ in ∇_2 taken $\lambda = \lambda_y$. For clarity, results of

only two cases are presented, i.e. $\lambda_y/\lambda_x = 0.5$ and purely longitudinal. For comparison the curve obtained for the isotropic case is also drawn. Figure 7 shows that for each λ_y/λ_x again a single curve is obtained but it is shifted to the left compared to the isotropic curve. The total shift going from isotropic to longitudinal however is limited and relatively small. It appears that the different results can be scaled onto a single line once again if they are presented as function of $f(r)\nabla_2$ with:

$$f(r) = e^{1-\frac{1}{r}} \tag{10}$$

with $r = \lambda_x/\lambda_y$. This is shown in Fig. 8. Thus, Eq. (6) accurately describes A_d/A_i if ∇_2 is replaced by $f(\lambda_x/\lambda_y)\nabla_2$, and $\lambda = \lambda_y$ is used in ∇_2.

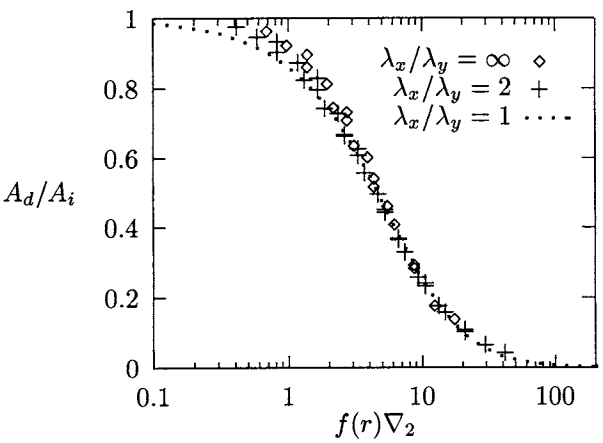

Figure 8. *A_d/A_i as a function of $f(\lambda_x/\lambda_y)\nabla_2$ with $\lambda = \lambda_y$. Anisotropic: $\lambda_x > \lambda_y$.*

6. Conclusion

Based on numerical simulations for many cases a simple relation is derived for the amplitude reduction of anisotropic harmonic surface patterns.

For isotropic waviness with $\lambda_x = \lambda_y = \lambda$ all amplitude reduction results fall onto a single curve using the dimensionless coordinate $\nabla_2 = (\lambda/b)(M^{1/2}/L^{1/2})$. For anisotropic waviness with $\lambda_y > \lambda_x$ an identical single curve was found when choosing the dimensionless coordinate ∇_2 with $\lambda = \lambda_x$, including the case of pure transverse waviness ($\lambda_y = \infty$). For anisotropic waviness with $\lambda_x > \lambda_y$, once again a reduction to a single curve was obtained when choosing as a dimensionless coordinate the product $\nabla_2\ f(\lambda_x/\lambda_y)$ using $\lambda = \lambda_y$ in ∇_2. This includes the stationary case of pure longitudinal waviness ($\lambda_x = \infty$) but to include this last case a generalisation of the definition of the deformed amplitude A_d was needed. All cases can be combined in a single equation:

$$\frac{A_d}{A_i} = \frac{1}{1 + 0.15\bar{f}(r)\nabla_2 + 0.015(\bar{f}(r)\nabla_2)^2} \tag{11}$$

where

$$\bar{f}(r) = \begin{cases} e^{1-\frac{1}{r}} & \text{if } r > 1 \\ 1 & \text{otherwise} \end{cases} \qquad \text{with} \quad r = \lambda_x/\lambda_y,$$

and

$$\nabla_2 = (\lambda/b)(M^{1/2}/L^{1/2}) \quad \text{with} \quad \lambda = \min(\lambda_x, \lambda_y)$$

REFERENCES

1. **Lubrecht, A.A.,** (1997), "Influence of Local and Global Features in EHL Contacts," Proc. 23rd Leeds-Lyon Symposium on Tribology, Ed. D. Dowson et al., Elseviers Tribology Series, **32**. pp. 17-25.
2. **Wedeven, L.D., and Cusano, C.,** 1979, "Elastohydrodynamic Film Thickness Measurements of Artificially Produced Surface Dents and Grooves," *ASLE Trans.*, **22**, 369-381.
3. **Kaneta, M., and Cameron, A.,** 1980, "Effects of Asperities in Elastohydrodynamic Lubrication," *ASME JOT*, **102**, 374-379.
4. **Kaneta, M.,** 1992, "Effects of Surface Roughness in Elastohydrodynamic Lubrication," *JSME*, III, **35**, 4, pp. 535-546.
5. **Kaneta, M., Sakai, T., and Nishikawa, H.,** 1992, "Optical Interferometric Observations of the Effects of a Bump on Point Contact EHL," *ASME JOT*, **114**, pp. 779-784.
6. **Kaneta, M., Sakai, T., and Nishikawa, H.,** 1993, "Effects of Surface Roughness on Point Contact EHL," *STLE Trib. Trans.*, **36,4**, pp. 605-612.
7. **Kaneta, J., Kanada, T., and Nishikawa, H.,** (1997), "Optical Interferometric Observations of

the Effects of a Moving Dent on Point Contact EHL," Proc. 23rd Leeds-Lyon Symposium on Tribology, Ed. D. Dowson et al., Elsevier Tribology Series **32**, pp. 69-79.

8. **Bush, A.W., and Skinner, P.H.,** (1982), "Surface roughness effects in Point Contact Elastohydrodynamic Lubrication, " *WEAR*, **83**, 285-301.
9. **Goglia, P.R., Cusano, C., and Conry, T.F.,** 1984, "The Effects of Surface Irregularities on the Elastohydrodynamic Lubrication of Sliding Line Contacts. Part I - Single Irregularities," *ASME JOT*, **106**, 104-112.
10. **Goglia, P.R., Cusano, C., and Conry, T.F.,** 1984, "The Effects of Surface Irregularities on the Elastohydrodynamic Lubrication of Sliding Line Contacts. Part II - Wavy Surfaces," *ASME JOT*, **106**, 113-119.
11. **Lubrecht, A.A., ten Napel, W.E., and Bosma, R.,** (1988), "The Influence of Longitudinal and Transverse roughness on the Elastohydrodynamic Lubrication of Circular Contacts," *ASME JOT*, **110**, 421-426.
12. **Barragan de Ling, FdM, Evans, H.P., Snidle, R.W.,** 1989, " Micro-Elastohydrodynamic Lubrication of Circumferentially Finished Rollers: The Influence of Temperature and Roughness," *ASME JOT*, **111**, pp. 730-736.
13. **Kweh, C.C., Evans, H.P., and Snidle, R.W.,** 1989, "Micro-Elastohydrodynamic Lubrication of an Elliptical Contact with Transverse and Three-Dimensional Roughness," *ASME JOT*, **111**, 577-583.
14. **Lee, R.T., and Hamrock, B.J.,** 1990, "A circular non-Newtonian Fluid Model: Part II - used in Micro-Elastohydrodynamic Lubrication," *ASME JOT*, **112**, 497-505.
15. **Venner, C.H., and ten Napel, W.E.,** (1992), "Surface Roughness Effects in an EHL Line Contact," *ASME JOT*, **114**, pp. 616-622.
16. **Ehret, P., Dowson, D., and Taylor, C.M.,** "Waviness Orientation in EHL Point Contact," (1996), Proc. 22nd Leeds-Lyon Symposium on Tribology, Ed. D. Dowson et al., Elsevier Tribology Series **31**, pp. 235-244.
17. **Chang, L., Cusano, C., and Conry, T.F.,** 1989, "Effects of Lubrication Rheology and Kinematic Conditions on Micro- Elastohydrodynamic Lubrication," *ASME JOT*, **111**, 344-351.
18. **Venner, C.H., Lubrecht, A.A., and ten Napel, W.E.,** (1991), "Numerical Simulation of the Overrolling of a Surface Feature in an EHL Line Contact," *ASME JOT*, **113**, pp. 777-783.
19. **Chang, L., and Webster, M.N.,** 1991, "A Study of Elastohydrodynamic Lubrication of Rough Surfaces," *ASME JOT*, **113**, 110-115.
20. **Chang, L.,** 1992, "Traction in Thermal Elastohydrodynamic Lubrication of Rough Surfaces," *ASME JOT*, **114**, 186-191.
21. **Osborn, K.F., and Sadeghi, F.,** 1992, "Time Dependent Line EHD Lubrication Using the Multigrid/Multilevel Technique", *ASME JOT*, **114**, 68-74.
22. **Ai, X., Cheng, H.S., and Zheng, L.,** 1993, "A Transient Model for Micro-Elastohydrodynamic Lubrication with Three-Dimensional Irregularities," *ASME JOT*, **115**, pp. 102-110.
23. **Ai, X., and Cheng, H.S.,** 1994, "The Influence of Moving Dent on Point EHL Contacts," *STLE Trib. Trans.*, **37**, pp. 323-335.
24. **Ai, X., and Cheng, H.S.,** 1994, "A Transient EHL Analysis for Line Contacts with a Measured Surface Roughness using Multigrid Technique,"
25. **Ai, X., and Cheng, H.S.,** 1996 "The Effects of Surface Texture on EHL Point Contacts," *ASME JOT*, **118**, pp. 59-66.
26. **Venner, C.H., and Lubrecht, A.A.,** 1994, "Transient Analysis of Surface Features in an EHL Line Contact in the case of Sliding," ASME JOT, **116**, pp. 186-193.
27. **Venner, C.H., and Lubrecht, A.A.,** 1994, "Numerical Simulation of a Transverse Ridge in a Circular EHL Contact, under rolling/sliding", ASME JOT, **116**, pp. 751-761.
28. **Venner, C.H., and Lubrecht, A.A.,** 1994, "Numerical Simulation of Waviness in a Circular EHL Contact, under rolling/sliding", Proc. 20nd Leeds-Lyon Symposium on Tribology, Ed. D. Dowson et al., Elsevier Tribology Series **30**, pp. 259-272.
29. **Couhier, F., Lubrecht, A.A., Nelias, D., and Flamand, L.,** 1996, "Influence of the Sliding Speed on the Elastohydrodynamically Lubricated Film Thickness Shape of Wavy Contacts," Proc. 22nd Leeds-Lyon Symposium on Tribology, Ed. D. Dowson et al., Elsevier Tribology Series **31**, pp. 515-526.
30. **Venner, C.H., and Lubrecht, A.A.,** 1996, "Numerical Analysis of the influence of Waviness on the Film Thickness of a Circular EHL Contact", ASME JOT, **118**, pp. 153-161.
31. **Ehret, P., Dowson, D., and Taylor, C.M.** "Time-Dependent Solutions with Waviness and

Asperities in EHL Point Contacts," Proc. 23rd Leeds-Lyon Symposium on Tribology, Ed. D. Dowson et al. Elseviers Tribology Series, **32**, pp. 313-324.

32. **Lubrecht, A.A., and Venner, C.H.**, 1992, "Aspects of Two-Sided Surface Waviness in an EHL Line Contact," Proc. 19th Leeds-Lyon Symposium on Tribology, Ed. D. Dowson et al., Elsevier Tribology Series, **25**, pp. 205-214.
33. **Venner, C.H., and Morales Espejel, G.E.**, "Amplitude Reduction of Small Amplitude Waviness in EHL Line Contacts", *Submitted to ImechE, Part J, Journal of Engineering Tribology.*
34. **Lubrecht, A.A.**, 1987, "Numerical Solution of the EHL Line and Point Contact Problem Using Multigrid Techniques," Ph.D. Thesis, University of Twente, Enschede, The Netherlands, ISBN 90-9001583-3.
35. **Lubrecht, A.A., Breukink, G.A.C., Moes, H., ten Napel, W.E., and Bosma, R.**, 1987, "Solving Reynolds' equation for EHL Line Contacts by Application of a Multigrid Method," Proc. 13th Leeds Lyon Symposium on Tribology, Elsevier Tribology Series **11**, Ed. D. Dowson et al., pp.175-182.
36. **Lubrecht, A.A., ten Napel, W.E., and Bosma, R.**, (1987), "Multigrid, an Alternative Method of Solution for Two-Dimensional Elastohydrodynamically Lubricated Point Contact Calculations," *ASME JOT*, **109**, 437-443.
37. **Venner, C.H.**, 1991, "Multilevel Solution of the EHL Line and Point Contact Problems," Ph.D. Thesis, University of Twente, Enschede, The Netherlands. ISBN 90-9003974-0.
38. **Greenwood, J.A., and Johnson, K.L.**, 1992, "The Behaviour of Transverse Roughness in Sliding Elastohydrodynamically Lubricated Contacts," *WEAR*, **153**, pp. 107-117.
39. **Morales Espejel, G.E.**, 1993, "Elastohydrodynamic lubrication of smooth and rough surfaces," PhD. Thesis, University of Cambridge, Department of engineering.
40. **Greenwood, J.A., and Morales Espejel, G.E.**, 1994, "The Behaviour of Transverse Roughness in EHL Contacts," *Proc. IMechE*, **208**, pp. 121-132.
41. **Greenwood, J.A., and Morales-Espejel, G.E.**, (1997), "The Amplitude of the Complementary Function for Wavy EHL Contacts," Proc. 23rd Leeds-Lyon Symposium on Tribology, Ed. D. Dowson, Elsevier Tribology Series, **32**, pp. 307-312.
42. **Couhier, F.**, 1996, "Influence des Rugosites de Surface sur les Mecanismes de Lubrification de Contact Elastohydrodynamique Cylindre-Plan", (in French) Ph.D. Thesis, INSA de Lyon, France.
43. **Venner, C.H., Couhier, F., Lubrecht, A.A., and Greenwood, J.**, (1997) "Amplitude Reduction of Waviness in Transient EHL Line Contacts," Proc. 1996 Leeds Lyon Tribology Conference, Elsevier Tribology Series **32**, Ed. Dowson et al., pp. 103-112.
44. **Lubrecht, A.A., Graille, D., Venner, C.H., and Greenwood, J.A.**, (1997), "Waviness Amplitude Reduction in EHL Line Contacts under Rolling-Sliding, " *ASME JOT*, in press.
45. **Hooke, C.J.**, 1997, "Surface Roughness Modification in Elastohydrodynamic Line Contacts operating in the elastic Piezoviscous Regime,", *Proc. Inst. Mech. Engrs Part J.*, V 212, *in press*
46. **Dowson, D., and Higginson, G.R.**, 1966, "Elastohydrodynamic Lubrication, The Fundamentals of Roller and Gear Lubrication," Pergamon Press, Oxford, Great Britain.
47. **Roelands, C.J.A.**, 1966, "Correlational Aspects of the Viscosity-Temperature-Pressure Relationship of Lubricating Oils" Ph.D. Thesis, Technical University Delft, Delft, The Netherlands, (V.R.B., Groningen, The Netherlands).
48. **Venner, C.H.**, "Higher Order Multilevel Solvers for the EHL Line and Circular Contact Problem," *ASME Journal of Tribology*, **116**, pp. 741-750.
49. **Lubrecht, A.A., and Venner, C.H.**, 1998, "Elastohydrodynamic Lubrication of Rough Surfaces, " *To appear in special issue of ImechE part J, Journal of Engineering Tribology.*
50. Private communication/discussion with Drs C.J. Hooke and J.A. Greenwood

A. Accuracy

For time dependent problems great care must be taken to obtain accurate results. Reynolds' equation in the high viscosity region reduces to an "advection-diffusion" equation:

$$\mathcal{F}_\epsilon - \frac{\partial(\bar{\rho}H)}{\partial X} - \frac{\partial(\bar{\rho}H)}{\partial T} = 0 \qquad (12)$$

where $\mathcal{F}_\epsilon$ symbolises a differential operator, i.e. in this case the poisseulle terms. The solution in the limit of small $\mathcal{F}_\epsilon$ is $\bar{\rho}H \approx (\bar{\rho}H)(X - T)$, i.e. variations of $(\bar{\rho}H)$ are propagated along the charac-

teristic $X = T$ without any change of amplitude. The solution for small $\mathcal{F}_\epsilon$ will show the same behaviour, except that the effect of a small viscous terms is that the amplitude of an oscillatory component in the solution will not be a constant but slowly decay, depending on the (local) value of $\mathcal{F}_\epsilon$. It can easily be shown that the solution to the discretised problem up to a higher order terms will satisfy:

$$\mathcal{F}_\epsilon - \frac{\partial(\bar{\rho}H)}{\partial X} - \frac{\partial(\bar{\rho}H)}{\partial T} + \tau^{\Delta_X,\Delta_T} = 0 \qquad (13)$$

where τ^{Δ_X,Δ_T} is the truncation error made in the discretisation. If this error is sufficiently small compared to $\mathcal{F}_\epsilon$ the discrete solution will mimic the physical behaviour of the continuous solution. However, if $\mathcal{F}_\epsilon$ is very small, as is the case in EHL the discrete solution may show viscous effects, e.g. amplitude reduction (or phase shift), caused by the truncation error, which are thus mesh size dependent. Indeed, with decreasing mesh size the truncation error decreases and eventually on very fine grids and using very small time steps one will converge to the right continuous solution, but this only occurs on grids where $\mathcal{F}_\epsilon$ starts to dominate τ. In fact, as long as this stage is not reached one simply obtains a solution for a case with much larger viscous effects than should occur for the given operating conditions. This for example shows up as amplitude decay in the solution as a function of space to an extend much larger than the real viscous term could ever account for. These effects will be very strong when a first order discretisation is used, see Venner [37][chapter 8], and [26]. Therefore, generally a second order discretisation should be used. A convenient choice is to separately discretise the wedge and squeeze term with the well known upstream second order discretisation, e.g. see [48, Appendix B], the so-called $SU2$ scheme (Standard Upstream 2nd Order).

In CFD many alternative discretisations for the advective part of (13) can be found. Of particular interest are the so-called narrow schemes. Instead of discretising both terms separately, the combined term $(\bar{\rho}H)_X + (\bar{\rho}H)_T$ is discretised using a given set of points and demanding a prescribed order of accuracy. Stability of the discretisation

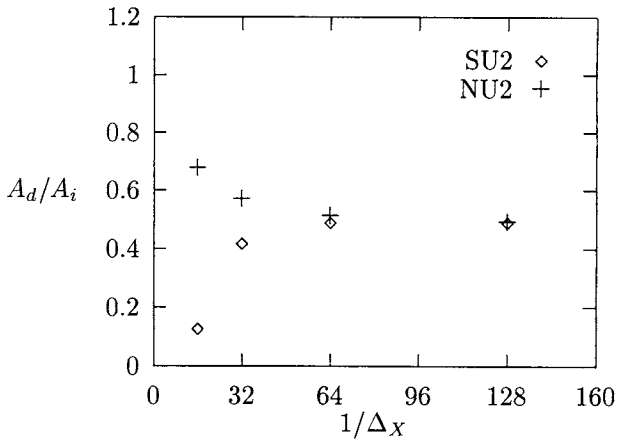

Figure 9. *A_d/A_i as a function of the mesh size (timestep) $M = 1007.6$, $L = 12.05$, and $\lambda_x/b = \lambda_y/b = 0.5$ ($\Delta_X = \Delta_Y = \Delta_T$).*

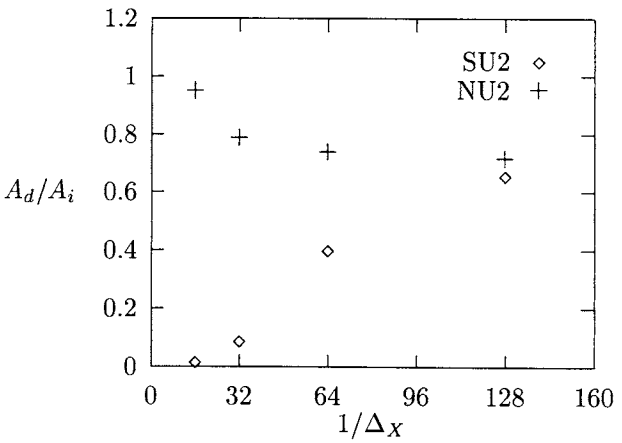

Figure 10. *A_d/A_i as a function of the mesh size (timestep) $M = 1007.6$, $L = 12.05$, and $\lambda_x/b = \lambda_y/b = 0.25$ ($\Delta_X = \Delta_Y = \Delta_T$).*

(not amplifying components in the solution) may then require the use of one or more stencils with angles smaller than 90 degrees, together covering all possible directions in the flow each in a manner as narrow as possible. This makes the discretisation formula a bit more complex, but this disadvantage is often outweighted by the gain in accuracy. An example of a second order discretisation thus derived is the narrow upstream scheme "NU2", see [33].

As an example Fig. 9 shows A_d/A_i as a function of the mesh size obtained with the $SU2$ and $NU2$ schemes for the load case displayed in Fig. 1 with $\lambda_x/b = \lambda_y/b = 0.5$. The figure shows that both schemes converge to the same value for sufficiently fine grids but, even though both schemes are second order, on coarser grids the result obtained with the $SU2$ scheme is less accurate. This effect will be stronger if the wavelength is smaller, see Fig. 10, where A_d/A_i as a function of the mesh size is shown for $\lambda_x/b = \lambda_y/b = 0.25$. For this case Fig. 11 and 12 show how the differences in accuracy show in the solution, i.e. in the film profile at the line $Y = 0$ as a function of X. Two effects can be observed. Firstly, with decreasing mesh size the level around which the film thickness oscillates converges in the same way as the central film thickness converges for the steady state solution. This behaviour, by definition, is the same for both the $NU2$ and $SU2$ results. Secondly, the amplitude of the oscillation itself converges. This latter behaviour is governed by the truncation error in the transient equation. Here the difference between the two schemes clearly shows. Even though the $SU2$ scheme is second order too, and also has a truncation error that vanishes for the characteristic component $X = T$ (for $\Delta_T = \Delta_X$), its results, for this high load and small wavelength case, exhibit an almost complete amplitude reduction on the coarsest grids. Only for $\Delta_X = 1/128$ it becomes small. The $NU2$ results are much more accurate. Even on the coarsest grids there is no amplitude reduction. However, on these grids there is a slight phase error (related to higher order terms in τ). Thus, compared with $SU2$ already on coarse grids it gives a good approximation to the appropriate "physical" behaviour of the continuous equations.

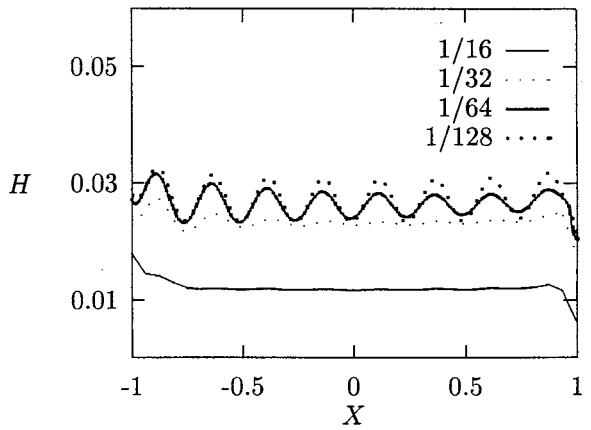

Figure 11. *Film thickness at the line $Y = 0$ as a function of X for $M = 1007.6$, $L = 12.05$, and $\lambda_x/b = \lambda_y/b = 0.25$ obtained using the $SU2$ scheme as a function of Δ_X ($\Delta_X = \Delta_Y = \Delta_T$).*

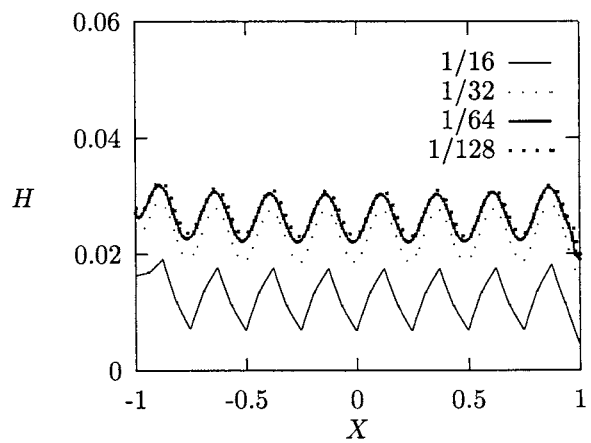

Figure 12. *Film thickness at the line $Y = 0$ as a function of X for $M = 1007.6$, $L = 12.05$, and $\lambda_x/b = \lambda_y/b = 0.25$ obtained using the $NU2$ scheme as a function of Δ_X ($\Delta_X = \Delta_Y = \Delta_T$).*